Egypt. J. Chem. **Vol. 63,** No. 4, pp. 1359 -1382 (2020)

Egyptian Journal of Chemistry
http://ejchem.journals.ekb.eg/

Facile Hydrothermal Synthesis of Sm and Eu doped TiO_2/Graphene Oxide Nanocomposites for Photocatalytic Applications

Mariam Sh. Gohr[1]*, Hoda S. Hafez[2], Mona M. Saif[3], Hesham M. A. Soliman[1] and Mohamed Sabry A. Abdel-Mottaleb[4]

[1]Nanotechnology and New Composite Materials Department Advanced Technology and New Materials Research Institute (ATNMRI), City of Scientific Research and Technological Applications (SRTA-City), New Bourg El-Arab City 21934, Alexandria, Egypt.

[2] Environmental Studies and Research Institute (ESRI), University of Sadat City (USC), Menofia, Egypt.

[3] Department of Chemistry, Faculty of Education, Ain Shams University, Roxy, 11341 Cairo, Egypt.

[4] Department of Chemistry, Faculty of Science, Ain Shams University, Abbassia, 11566 Cairo, Egypt.

LANTHANIDE (Ln3+) doped TiO_2 supported on Graphene oxide (GO) (Ln^{3+} =Eu^{3+} and Sm^{3+} ions) were prepared by using a low cost and facile hydrothermal method. Structural, morphological and optical properties of the un-doped and Ln^{3+}-doped nanocomposites were characterized by X-ray diffraction (XRD), scanning electron microscopy (SEM) equipped with energy dispersive X-Ray (EDX), transmission electron microscopy (TEM), (SBET) Barrett–Joiner–Halenda surface area analysis, Fourier transform infrared spectroscopy (FTIR), Raman spectroscopy (RS) and diffuse reflection spectrometry (DRS). The photocatalytic activities of the catalysts were investigated by studying photo decolorization and photodegradation of Methylene Blue (MB). The XRD results showed that all the TiO_2 prepared samples exhibit anatase phase and no other peaks have been observed indicating the absence of impurities in the prepared samples. SEM images demonstrated that the TiO_2 nanoparticles are well dispersed on the GO surface. A red shift in the UV-Vis absorption of the prepared samples have been observed suggesting the charge transfer between the dopants and TiO_2. The photocatalytic activity results showed that 0.015 mol% Eu^{3+}-doped TiO_2/GO nanocomposite possesses the highest photocatalytic activity. Chemical oxygen demand (COD) analysis indorsed the photodegradation results. This promising photocatalyst led to almost complete mineralization of MB dye after only 90 min upon expose to UV light. The results clearly demonstrated the beneficial role of both GO as a supporting material and lanthanide metal ions as dopants on the degradability of MB.

Keywords: Photocatalysis, Lanthanide doped Titania, Graphene oxide, Methylene blue (MB), UV light.

Introduction

Environmental contaminations as wastewater and air pollution have become a very serious problem, the world is facing today. For water treatment, photocatalysis is one of the most powerful and environment friendly techniques [1,2]. Titanium dioxide is one of the most promising semiconductors that have been widely studied because of its unique photoelectric properties, high chemical stability, non-toxicity and low cost [3]. It has been reported that anatase phase is more photoactive than rutile or brookite forms because of the low recombination rate of its photogenerated electrons and holes on the surface

*Corresponding author e-mail: mariam.gohr@gmail.com. Tel. 01288715588
Received 22/07/2019; Accepted 02/09/2019
DOI: 10.21608/ejchem.2019.15112.1914

of TiO_2. Despite its role as a good photocatalyst semiconductor material its efficiency is limited by its wide bandgap and the fast electron–hole recombination [4]. A lot of approaches have been studied to extend the optical absorption of TiO_2 into the visible light region, aiming to modify its photocatalytic activity. One of these approaches is doping. The photocatalytic activity of TiO_2 can be increased by doping with Lanthanide elements [5-8]. Because of their unique 4*f* electronic configuration and spectral characteristics, lanthanides are ideal elements for modifying the crystal structure, electronic structure, optical properties, surface adsorption of TiO_2 and forming a series of novel promising photocatalysts [5]. Lanthanides provide an opportunity for an in-depth study of the electronic structure that can enhance the photocatalytic activity of TiO_2 [9,10]. In addition, it has been found that loading TiO_2 nanoparticles on a mesoporous material as zeolites, alumina, silica or carbon-based materials can also enhance the photocatalytic activity of TiO_2 [11-14]. Carbon is used as support material for catalysts because of its high surface area [15]. Carbon nanomaterials, such as carbon nanotubes (CNTs) and graphene oxide (GO) increase the surface area of TiO_2 for trapping more organic pollutants and enhance the rate of photocatalytic process [16].

In the present work, we have investigated a simple hydrothermal procedure for the preparation of some lanthanide doped TiO_2 nanomaterials that are decorated on GO forming a new composite nanomaterial (Sm^{3+} and/or Eu^{3+}-doped TiO_2/GO). The new catalysts would be characterized by standard techniques. Its potential applications as photocatalysts were also studied. As a test material we have chosen MB dye, which is considered as a model organic dye pollutant that may exist in water.

Experimental

Materials and Reagents

All chemicals and reagents were of analytical purity and used without any additional purification. Graphite flakes, hydrochloric Acid 37%, sulphuric Acid 98%, potassium permanganate ($KMnO_4$), hydrogen peroxide 30%, Titanium (IV) isopropoxide ($Ti(OC_3H_7)_4$ (99%)), Methylene blue (MB), Samarium (iii) nitrate hexahydrate ($Sm(NO_3)_3 \cdot 6H_2O$), Europium (iii) nitrate pentahydrate ($Eu(NO_3)_3 \cdot 5H_2O$), isopropanol (C_3H_8O (99%)) and ethanol (C_2H_5OH (99%)) were purchased from Sigma-Aldrich, Sigma-Aldrish Chemie Gmbh, Taufkirchen, Germany. The chemical structure of MB dye is shown in Fig. 1. Deionized (DI) water was used throughout this work.

Preparation Methods

Graphene oxide sheets (GO) were prepared from graphite powder by improved Hummer method as previous paper reported [17]. Ln(III)-TiO_2/GO were prepared by adding 30 mg GO in 25 mL isopropanol and sonicated at room temperature for 90 min to ensure the dispersion of graphene oxide in the alcoholic solution. Then, a certain amount of titanium isopropoxide was added into the solution and kept stirring for 10 min. Then 1 mL of water containing an appropriate amount of the dopant metal ions (Eu^{3+}or Sm^{3+}) was added dropwise to the above solution with different molar ratios ranging from (0.01 to 0.03 mol% relative to TiO_2). The resulting mixture transferred into a 100 mL Teflon lined autoclave and heated at 180 ºC for 0.5 h. The resulting powder was washed by ethanol for several times and then dried at 50 ºC overnight. Pure TiO_2 and TiO_2/GO (1:100) were prepared under the same conditions without the addition of the lanthanide metal ions.

Characterization

X-ray diffraction (XRD) patterns were investigated by the X-ray diffractometer (X-ray 6100 Shimadzu-Japan) with Cu Kα radiation (λ= 0.15406) with Kβ filter at 30 kV and 30 mA. The Bragg angle (2θ) had the range from 10º - 80º and scan rate 5 º/min. The morphologies were characterized by a scanning electron microscope (SEM) (JEOL JSM 6360LA, Tokyo, Japan). The samples were coated with gold using sputtering coater (model: S150B, Edwards High Vacuum Ltd., England) in order to avoid the buildup of local electrical charges. SEM instrument equipped with Energy dispersive X-ray (EDX, Oxford Instruments NanoAnalysis, Concord, MA, USA, Shimadzu, Kyoto-Japan. PG Instruments Ltd, Woodway Lane, Alma Park, Leicestershire LE17 5FB, UK. Edwards High Vacuum Ltd, The Hamlyn Centre Bessemer Building,South Kensington Campus, Imperial College London, London, UK) for semi-quantitative elemental analysis of the prepared samples. Transmission electron spectroscopy (TEM) was performed

with a JEOL JEM 100CX, Tokyo, Japan. Optical properties of the prepared samples were investigated using UV-Vis diffuse reflectance spectroscopy on a Shimadzu UV-2550 (Japan). $BaSO_4$ was used as the reflectance standard. The Brunauer–Emmett–Teller (BET) specific surface area (S_{BET}) was determined by a multipoint BET method using the adsorption data in the relative pressure (P/P_o) range of 0.05–0.25. Desorption isotherm was utilized to measure the distribution of pore sized using the Barret–Joyner–Halender (BJH) method [18]. The nitrogen adsorption volume in the relative pressure was utilized to measure the average pore size and the pore volume. The IR spectra were recorded on FTIR spectrometer (8400s, Shimadzu, Japan) using KBr disc method while the sample's Raman spectra were investigated by using Raman spectroscopy (BRUKER, OPTIK, GMBH, Senterra, Germany). The UV-Vis absorption spectrum of the prepared samples and the concentration of MB dye were determined by a UV-Visible spectrophotometer ($T80^+$, PG instruments Ltd., UK). The total organic carbon obtained from the photodegradation of the organic dyes was measured by a Multi parameter Bench Photometer with chemical oxygen demand (COD) and accompanied with COD test tube bench heater model C-99 from HANNA Company 270 George Washington Hwy, Smithfield, RI 02917, USA.

Photocatalytic Activity

The photodegradation experiments of the prepared samples were carried out in a Home-made UV-A photoreactor with a UV-light intensity of 3 $mW.cm^{-2}$. Briefly, 100 mL dye solutions were prepared in appropriate concentrations using bi-distilled water. Dye solutions were stirred in the dark for 30 min after the addition of 50 mg of the catalyst to establish an adsorption/desorption equilibrium. Samples of suspension were withdrawn at regular intervals and were immediately centrifuged at 10000 rpm for 5 min to remove the catalyst particles completely. The progress of the photocatalytic decolorization was monitored by measuring the absorbance of the solution samples at the maximum wavelength of MB dye (664 nm). The total mineralization test was examined by measuring the COD of the samples before and after UV-light irradiation.

Result and Discussion

Morphological and Crystallographic Characterization

XRD characterization is an effective and useful technique to determine the crystallite phase and the size of the nanomaterials. The XRD patterns of GO, TiO_2, TiO_2/GO (1:100) and Sm^{3+} and Eu^{3+}-doped TiO_2/GO (0.015 mol %) nanocomposites are shown in Fig. 2. XRD pattern of GO (Fig. 2a) shows two distinct peaks at $2\theta = 10.6^o$ and 42.5^o, which are assigned to (0 0 2) and (1 0 0) crystallographic planes of the carbon hexagonal structure. The interlayer spacing value for GO is 0.83 nm. The distance between consecutive carbon layers is increased indicates the successful oxidation of the starting graphite [19]. XRD pattern of pure TiO_2 nanoparticles (Fig. 2b) is well ascribed to the standard powder diffraction pattern of anatase TiO_2 (JCPDS No. 21–1272) [20]. In the un-doped and doped-TiO_2/GO nanocomposite system (Fig. 2c-e), no other diffraction peaks are assigned for GO or the dopant (Sm^{3+} or Eu^{3+} oxides). This firstly confirms that the C atoms are completely replace some of the oxygen atoms in the TiO_2 crystal lattice in the TiO_2/GO composite indicating that no GO is left on the catalyst's surface. This confirms that GO is in a high dissolution state in the TiO_2 lattice rather than an isolated species on the surface of TiO_2 [21]. This may be due to the low amounts of GO (1%) and the dopant ion concentrations (0.015%) in the samples. The average crystallite size of the prepared samples are calculated by using Debye-Scherer formula [22]. The average crystallite size of the prepared samples are given in Table 1.

$$d = \frac{k\lambda}{B\cos\theta} \qquad \textbf{(1)}$$

where d is the crystallite size, k is a constant of 0.9, λ is the X-ray wavelength of Cu which is 1.5406 Å, is the Bragg angle in degree and B is the full width at half maximum (FWHM) of the peak. Due to the much lower crystalline extent of graphene than that of TiO_2, it has been observed that the crystallite size of the prepared samples decrease after being doped with lanthanides [23-24]. This may be due to the segregation of the doping ions at the grain boundary. In turn, due to bigger ionic radii of Sm^{3+} (1.086 Å) and Eu^{3+} (1.036 Å) than Ti^{4+} (0.068 Å), it is difficult for Sm^{3+} and Eu^{3+} to replace Ti^{4+} in the crystalline lattice [6].

The morphology of GO, TiO_2, TiO_2/GO (1:100) and Sm^{3+} and Eu^{3+}-doped TiO_2/GO (0.015 mol%) photocatalysts are shown in Fig. 3 and Fig. 4. The SEM image of GO (Fig. 3a) shows a porous sponge-like structure with the graphene sheet not well connected together. This is an indication that the graphite has been exfoliated during the oxidation process. This also may be due to the distorted graphene sheets when oxygen and other functionality groups are attached to the sheets of graphene to form GO [25].The SEM image of TiO_2 (Fig. 3b) shows small spherical distributed TiO_2 particles. The SEM images of undoped and doped TiO_2/GO composite (Fig. 3c-e) demonstrate that the TiO_2 nanoparticles are well dispersed on the GO surface. The TiO_2 nanoparticles are attached onto the surface of GO sheets and they are intercalated between the graphene oxide ''Sandwich'' constructed in an aggregation [26]. These images show the presence of TiO_2 agglomerates. Due to the high amount of TiO_2 compared with the GO, the latter are less visible [27].

The TEM images of pure GO and TiO_2/GO are shown in Fig. 4(a,b), respectively. The regular shapes of TiO_2 with good defined boundaries and uniform size distribution, show a successful preparation method. The TEM study displays that the size of the TiO_2 nanoparticles are in the range of 6–12 nm with an average size of 9 nm. The TEM image of the TiO_2/GO (Fig. 4b) shows that there is a complete bounding between TiO_2 nanoparticles with wide distribution on very thin and transparent graphene oxide sheet. Figs. 4c and 4d show the TEM images of Sm^{3+} and Eu^{3+}-doped TiO_2/GO, respectively. The TiO_2 nanoparticles are found to be completely embedded into the GO sheets. Therefore, good contact and interaction between lanthanide-doped TiO_2 nanoparticles and GO has been achieved during the hydrothermal process, which is believed to be favorable for transferring the photogenerated electrons into a Ln(III) doped-TiO_2/GO composites during the photocatalytic process.

The elemental compositions of the prepared samples have been done by EDX analysis (Supplement1). The results confirm the presence of Ti, Sm, Eu, O and C. Also, the spectra indicate that the principal constituents are Ti and O with low concentrations of lanthanide ions and GO, as well as the obtained samples are free from impurities [21].

Optical Characterization

The FTIR spectra of GO, TiO_2, TiO_2/GO (1:100) and Sm^{3+} and Eu^{3+}-doped TiO_2/GO (0.015 mol%) nanocomposites are shown in Fig. 5. The FTIR spectrum of GO contains the characteristic peaks of GO at 3453 and 1087.9 cm^{-1}, due to O-H and C-O stretching vibrations, respectively. The peaks at 1626.1 cm^{-1} and 1722.5 cm^{-1} are due to C=O stretching vibration in the carboxylic acid group. The peak at 1400.4 cm^{-1} is due to C=C stretching vibration from un-oxidized sp^2 C-C bonds. The peak at 2348.1 cm^{-1} is due to O=C=O stretching vibration [18]. FTIR results of the present study are consistent with previous reports [21, 28]. The presence of polar oxygen containing functional groups strongly changes the Vander Waals interactions between GO layers and makes them hydrophilic. Due to the hydrophilic nature, GO can easily be dispersed in water and forms a stable colloidal aqueous suspension [29]. The FTIR spectra of the TiO_2, un-doped and Ln^{3+}-doped TiO_2/GO show a broad band about 3406 cm^{-1}which is assigned to the OH stretching frequency from the surface hydroxyl groups. The band at 1633 cm^{-1} corresponds to Ti–O–C vibration, which may result from the interaction between the surface hydroxyl groups of TiO_2 and the functional groups of graphene oxide. The bands observed in the region below 700 cm^{-1} are characteristic to the Ti-O vibration modes of the Ti^{3+}-O-Ti^{4+} in TiO_2. These results show the chemical coupling of TiO_2 and GO [30]. The peak at 1634 cm^{-1} is assigned to the bending vibrations of adsorbed water molecules [31]. The observed peak at 1415 cm^{-1}, which is due to C=C stretching vibrations from unoxidized graphene domains, is dominant for the TiO_2-GO samples [32]. Furthermore, no residual alkoxy peaks have been observed indicating the absence of impurities in the samples.

The typical Raman spectrum of GO, obtained at an excitation wavelength of 517 nm, is shown in Fig. 6a. The D peak at 1348 cm^{-1}, with an intensity comparable to the G peak at 1592 cm^{-1}, along with their large band width are indicative of significant structural disorder in GO [17]. Fig. 6 (b-e) shows the Raman spectra of the TiO_2, un-doped and Ln^{3+}-doped TiO_2/GO prepared by using the hydrothermal method. The Raman active peaks at 143 cm^{-1} (E_g), 395 cm^{-1} (B_{1g}), 515 cm^{-1} (A_{1g}), and 638 cm^{-1} (E_g) modes are for the as-prepared composites indicate the anatase structure of TiO_2. The (E_g) modes for all prepared composites were broader and blue-shifted from

144 cm^{-1} to 153 cm^{-1}. The peak shift of TiO_2, which appeared in the Raman spectrum is due to the doping with lanthanide [6]. The 1343 cm^{-1} and 1602 cm^{-1} modes are referred to the D and G bands of GO, respectively [17].

The light absorption characteristics of the obtained samples are investigated in Fig. 7. Fig. 7(a,b) shows the UV-Vis diffuse reflectance spectra for the TiO_2, TiO_2/GO and Ln^{3+}-doped TiO_2/GO with different lanthanide metal ions (Eu^{3+} and Sm^{3+}) concentrations ranging from 0.01 to 0.03 molar ratios. It may be seen very well that the undoped TiO_2/GO and Ln^{3+}-doped TiO_2/GO (with different Sm^{3+} and Eu^{3+} molar ratios) nanocomposites experienced increased light absorption in the visible range showing a red shift in the absorbance compared with the bare TiO_2. This can be attributed to the charge transfer between the dopant (f electrons of lanthanides and/or p electrons of carbon) and the TiO_2 conduction or valence band. As a result, the un-doped and Ln^{3+}-doped TiO_2 can absorb lower photo energy and this leads to higher photocatalytic activity. The band gap energies (E_g) of the prepared samples are calculated using Tauc's equation;

$$\alpha h\nu = B(h\nu - E_g)^{n/2} \qquad \textbf{(2)}$$

where α, ν, and B are the absorption coefficient, the light frequency and proportionality constant, respectively [33]. The value of n depends on the characteristics of the transition in the semiconductor. The Eg values are calculated by the extrapolation of the linear parts of the curves (Fig. 7c,d) and listed in Table 2.

BET Surface Area Analysis

The textural properties of as-prepared TiO_2, TiO_2/GO, Sm^{3+}-doped TiO_2/GO and Eu^{3+}-doped TiO_2/GO nanocomposite samples have been investigated using Brunauer–Emmett–Teller (BET) analysis. The BET surface area S_{BET}, total pore volume (V_t) and the mean pore volume of the samples are calculated and presented in Table 1. From the data in Table 1, it has been observed that doping with Sm^{3+} and Eu^{3+} leads to an increase of the total surface area of the TiO_2/GO composite. This will be favorable for photocatalytic applications, as the higher specific surface area of the photocatalysts doped with Ln(III) lead to increase the adsorption of more dye particles on its surface. This demonstrates that Ln(III) doped TiO_2 supported on GO composites are excellent candidate for adsorption and photocatalysis.

Photocatalytic Activity

The photocatalytic activities of the as-synthesized undoped and Ln(III)-doped TiO_2/GO (with different Ln(III) molar ratios) nanocomposite compared with that of the pure TiO_2 as a photocatalysts are tested on the degradation of MB as a model for an organic pollutant. Fig. 8(a-d) shows the visible absorption spectra of degraded MB over TiO_2, TiO_2/GO, 0.015 mol% Sm^{3+}- TiO_2/GO and 0.015 mol% Eu^{3+}- TiO_2/GO photocatalysts, respectively after exposure to UV-light illumination. It can be observed that the absorption peak intensity of MB at 664 nm decreases with the exposure time increasing, thus showing the decolorization of MB by the photocatalysts under investigation.

The decolorization rate kinetics of MB dye is found to obey first order rate kinetics confirmed by the linear fit eq. (3)

$$\ln A_t = \ln A_o - kt \qquad \textbf{(3)}$$

where k is the rate constant (min^{-1}), t is the irradiation time, $A_{t\ and}$ A_o are the initial and final absorption values of the dye solution, respectively. A plot of ln (A_t /A_o) versus t yields a straight line. The photocatalytic initial decolorization rate kinetics of MB with the different photocatalysts under investigation are shown in Fig. 9(a,b) and summarized in Table 2. The results demonstrated that all Ln(III)–TiO_2/GO catalysts achieved higher rates of MB degradation than the pure TiO_2 and TiO_2/GO catalysts. Moreover, it can be clearly seen that increasing the lanthanide dopant ion concentration leads to an increase of the photodegradation rate of MB till an optimum concentration (0.015 mol%). However, further increase in the lanthanide metal ion concentration, as a dopant metal ion, leads to retardation in the photo degradability of the dye solution (Fig. 9(c,d)).

This can be explained that below an optimum dopant metal ion concentration, the dopant acts as a charge carrier separator which increases the charge separation and enhances the photocatalytic performance of the nanocomposite. However, at higher metal concentration, the dopant can act as a charge recombination center which prevents the separation of the photogenerated charge carriers and furthermore represses the generation

TABLE 1: XRD and S_{BET} analysis of pure TiO_2, TiO_2/GO, 0.015% Sm-TiO_2/GO and 0.015% Eu-TiO_2/GO

Sample	Crystal Size (nm)	S_{BET} ($m^2.g^{-1}$)	V_t x 10^{-1} $cc.g^{-1}$	Average pore size (nm)
TiO_2	6.6	172	0.3596	8.3631
TiO_2/GO	5.4	212	0.2862	5.3972
0.015% Sm- TiO_2/GO	4.9	213	0.5543	10.405
0.015%Eu- TiO_2/GO	5.4	249	1.0499	16.815

TABLE 2: Absorption edge, band gap values and initial rate constants of MB dye (k) with TiO_2, TiO_2/GO and different x mol% of Ln(III)-doped TiO_2/GO catalysts

Sample	Optical characterization		Photocatalytic Activity	
	Absorption edge (nm)	Band gap (eV)	k 10^{-3}×(min^{-1})	R
TiO_2	383.9	3.23	3.30	0.98419
TiO_2/GO	413.3	3.00	9.10	0.99188
0.01% Sm- TiO_2/GO	387.5	3.21	13.2	0.99758
0.015% Sm- TiO_2/GO	376.8	3.29	17.1	0.99935
0.025% Sm- TiO_2/GO	374.6	3.31	15.1	0.99750
0.03% Sm- TiO_2/GO	372.4	3.33	11.5	0.99876
0.01% Eu- TiO_2/GO	380.4	3.26	14.9	0.99755
0.015% Eu- TiO_2/GO	372.4	3.33	25.6	0.99781
0.025% Eu- TiO_2/GO	381.5	3.25	22.5	0.99574
0.03% Eu- TiO_2/GO	370.1	3.35	16.5	0.99950

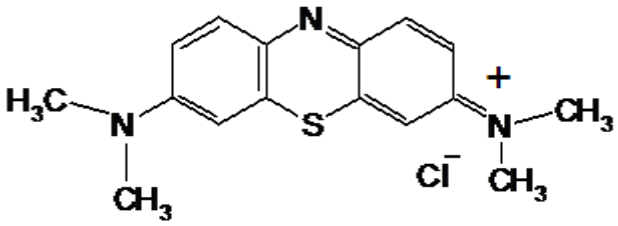

Fig. 1: The Chemical structure of MB dye

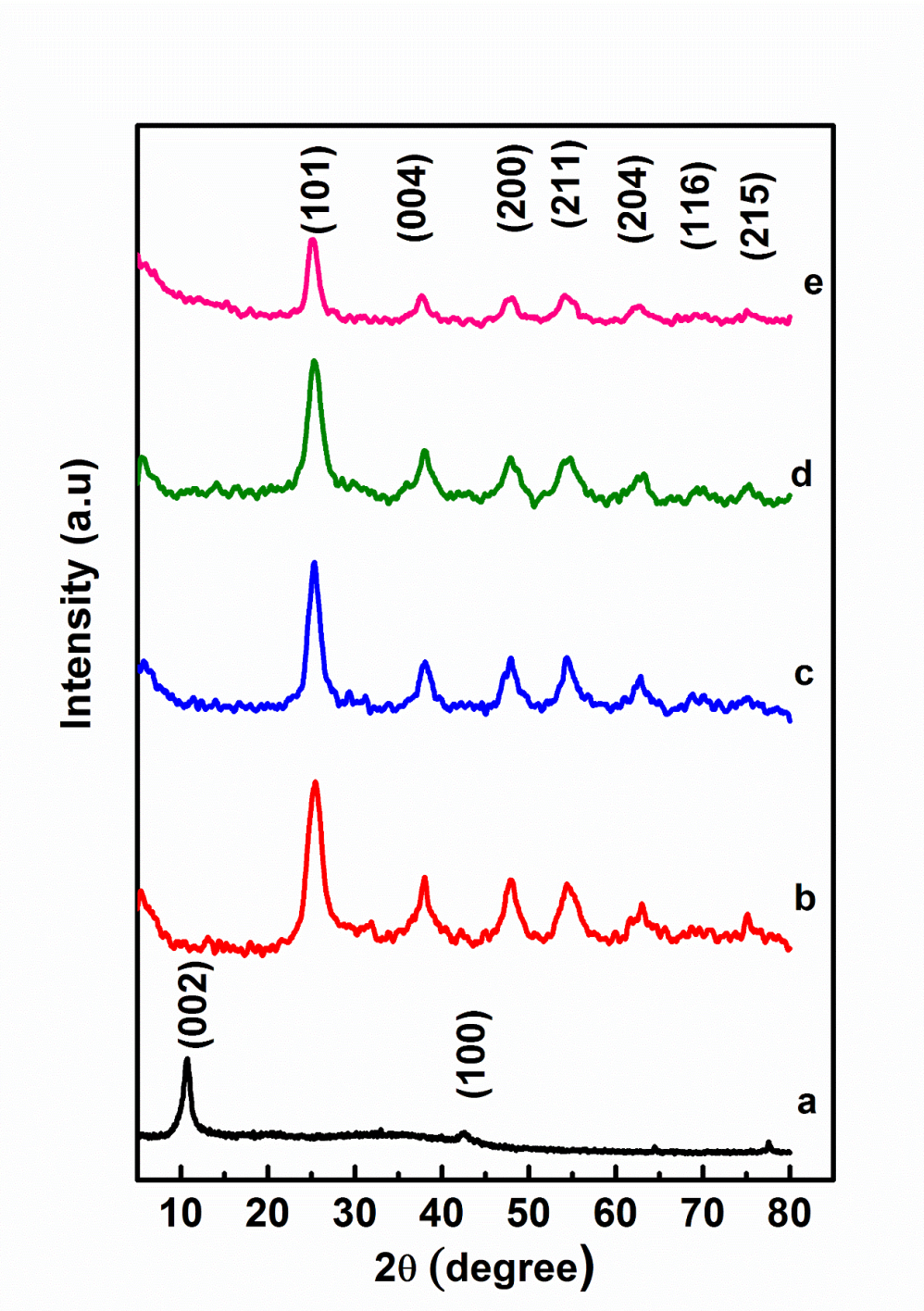

Fig. 2: XRD patterns of a) GO, b) TiO_2, c) TiO_2/GO, d) 0.015% Sm-TiO_2/GO and e) 0.015% Eu-TiO_2/GO

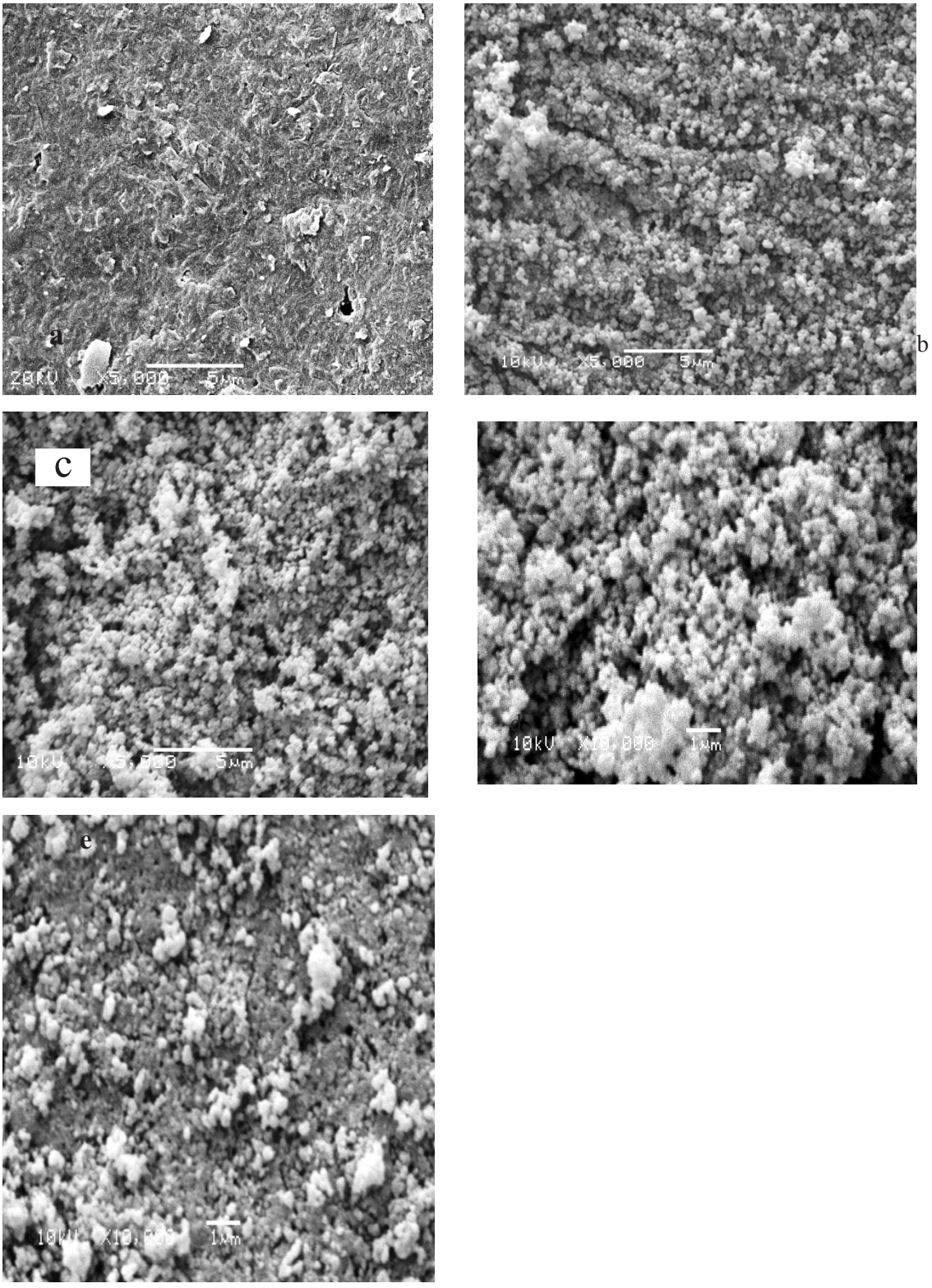

Fig. 3: SEM images of a) GO, b) TiO_2, c) TiO_2/GO, d) 0.015% Sm-TiO_2/GO and e) 0.015% Eu-TiO_2/GO

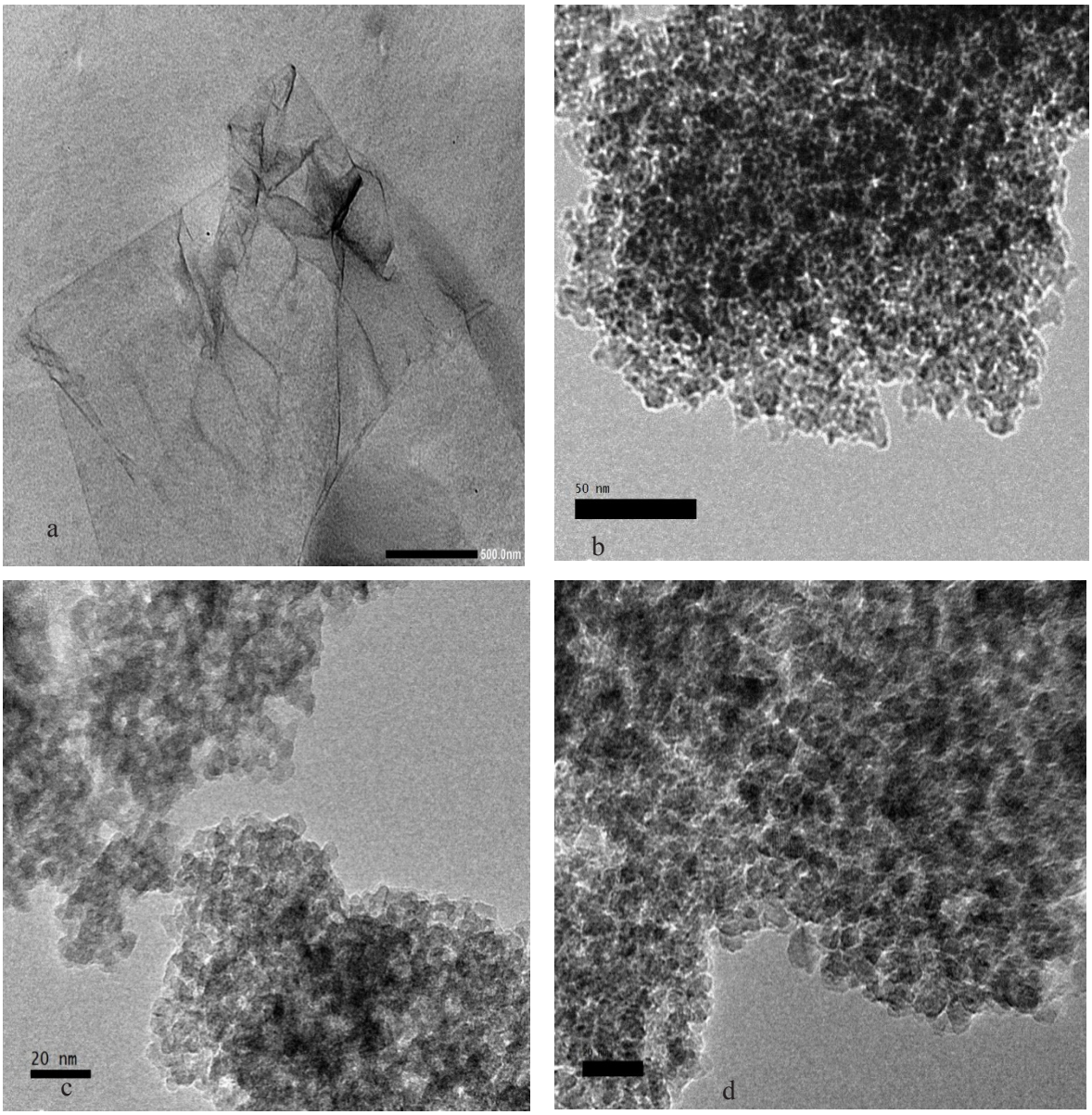

Fig. 4: TEM images of a) GO, b) TiO_2/GO, c) 0.015% Sm-TiO_2/GO and d) 0.015% Eu-TiO_2/GO

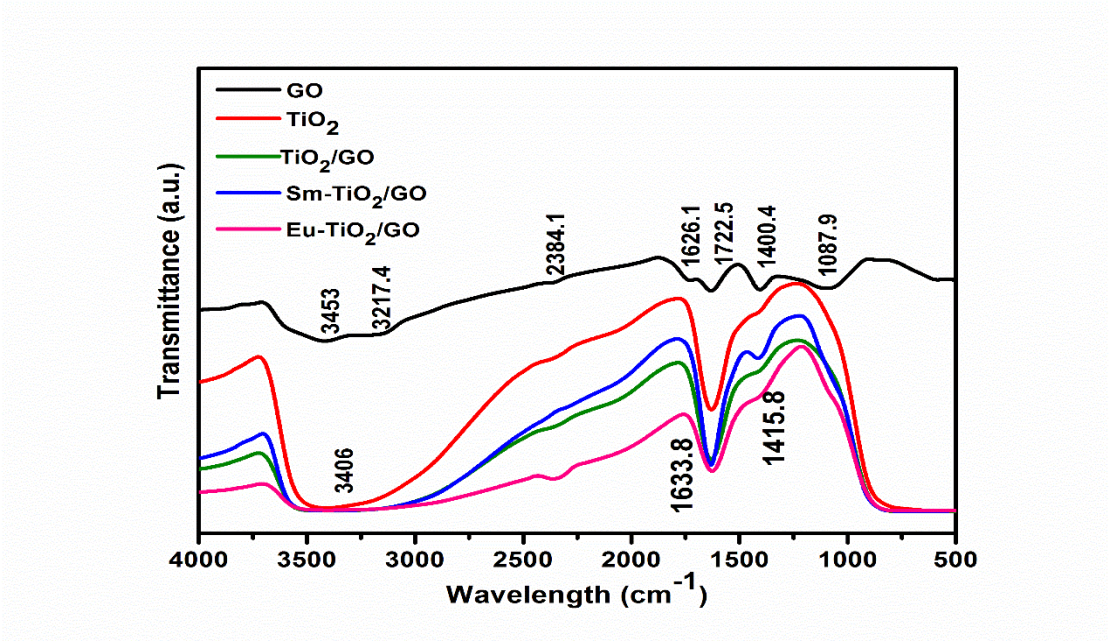

Fig. 5: FTIR spectra of GO, TiO_2, TiO_2/GO, 0.015% Sm-TiO_2/GO and 0.015% Eu-TiO_2/GO

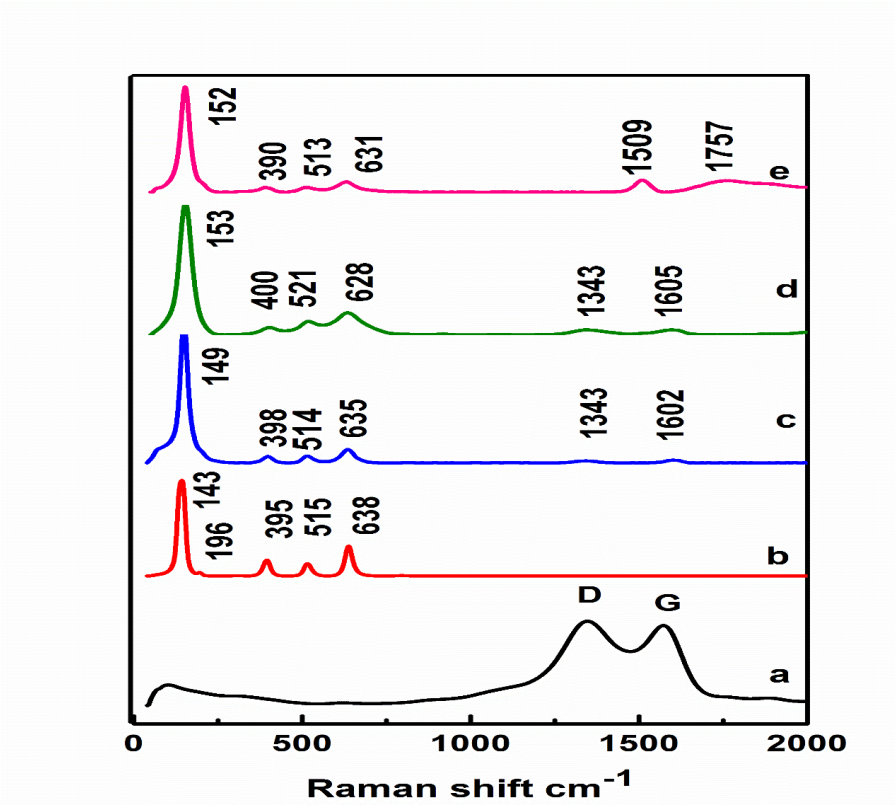

Fig. 6: Raman spectra of a) GO b) TiO_2, c) TiO_2/GO, d) 0.015% Sm-TiO_2/GO and e) 0.015% Eu-TiO_2/GO

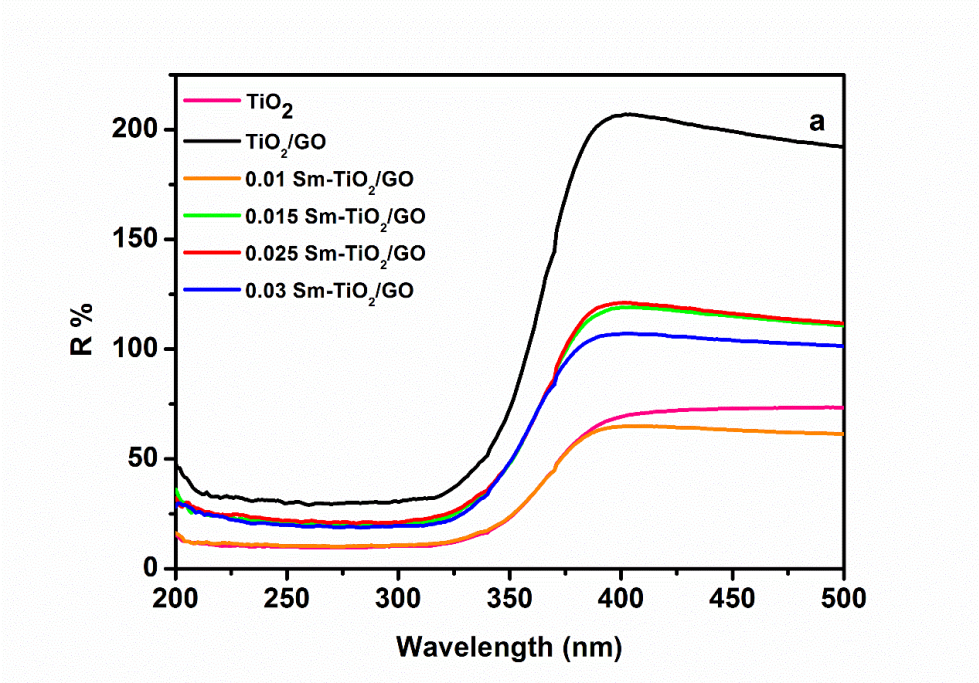
a
TiO2
TiO2/GO
0.01 Sm-TiO2/GO
0.015 Sm-TiO2/GO
0.025 Sm-TiO2/GO
0.03 Sm-TiO2/GO
R %
Wavelength (nm)

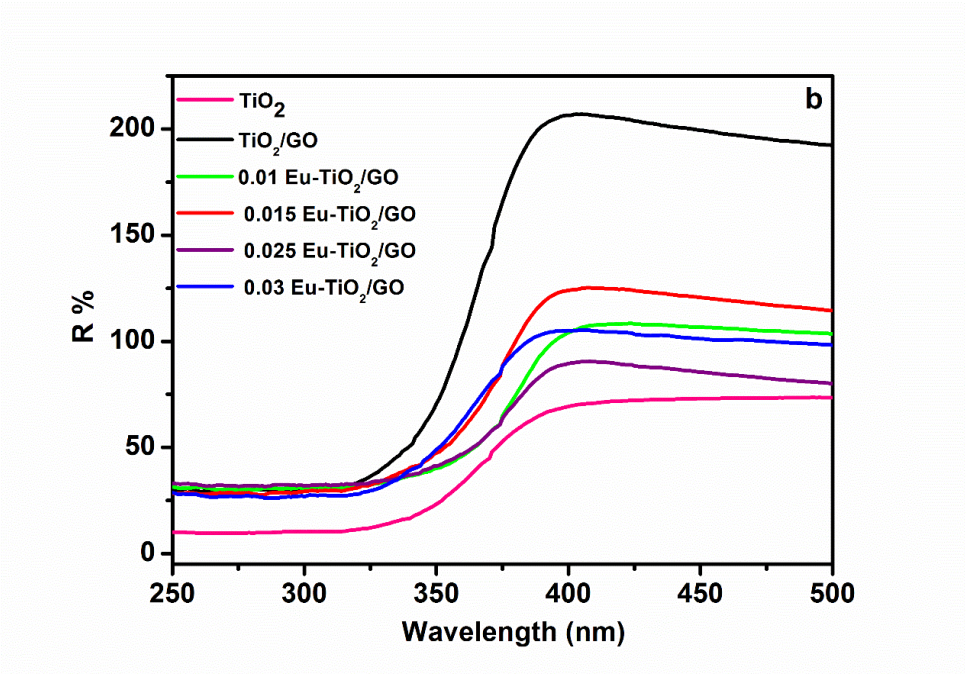
b
TiO2
TiO2/GO
0.01 Eu-TiO2/GO
0.015 Eu-TiO2/GO
0.025 Eu-TiO2/GO
0.03 Eu-TiO2/GO
R %
Wavelength (nm)

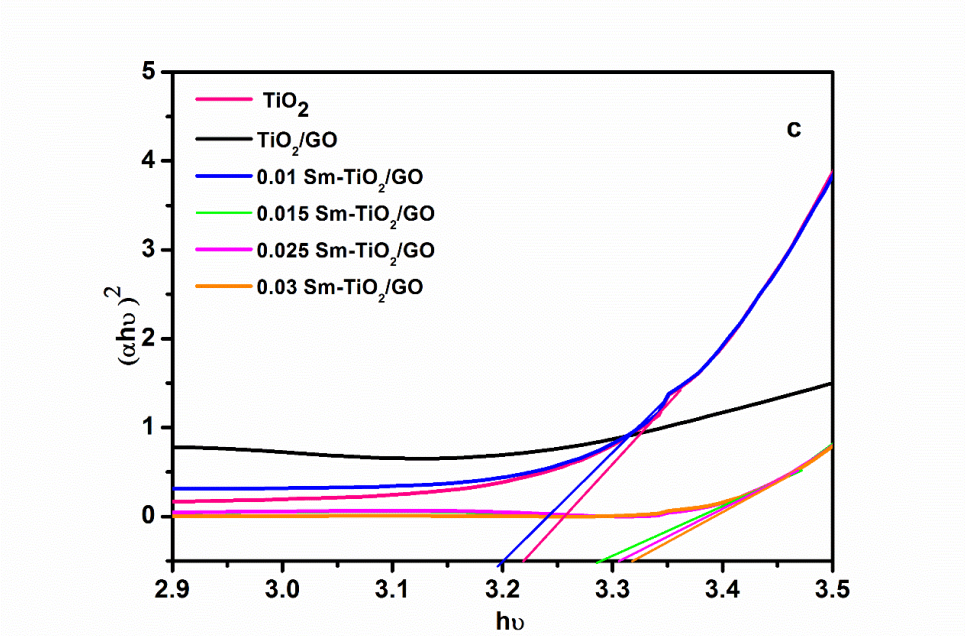

Fig. 7(a, b) UV-Vis diffuse reflectance spectra of TiO_2, TiO_2/GO and different x mol % Ln(III) doped TiO_2/GO catalysts; (c, d) Tauc plot of TiO_2, TiO_2/GO and different x mol % Ln(III) dopedTiO_2/GO cataly

z

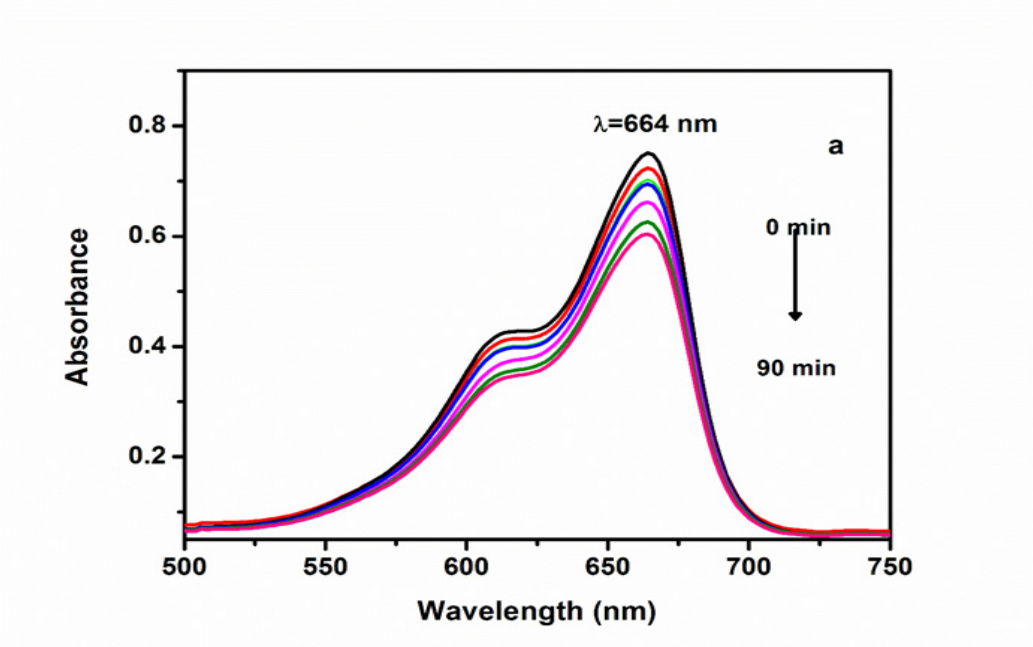
λ=664 nm
a
0 min
90 min
Absorbance
Wavelength (nm)
0.8
0.6
0.4
0.2
500
550
600
650
700
750

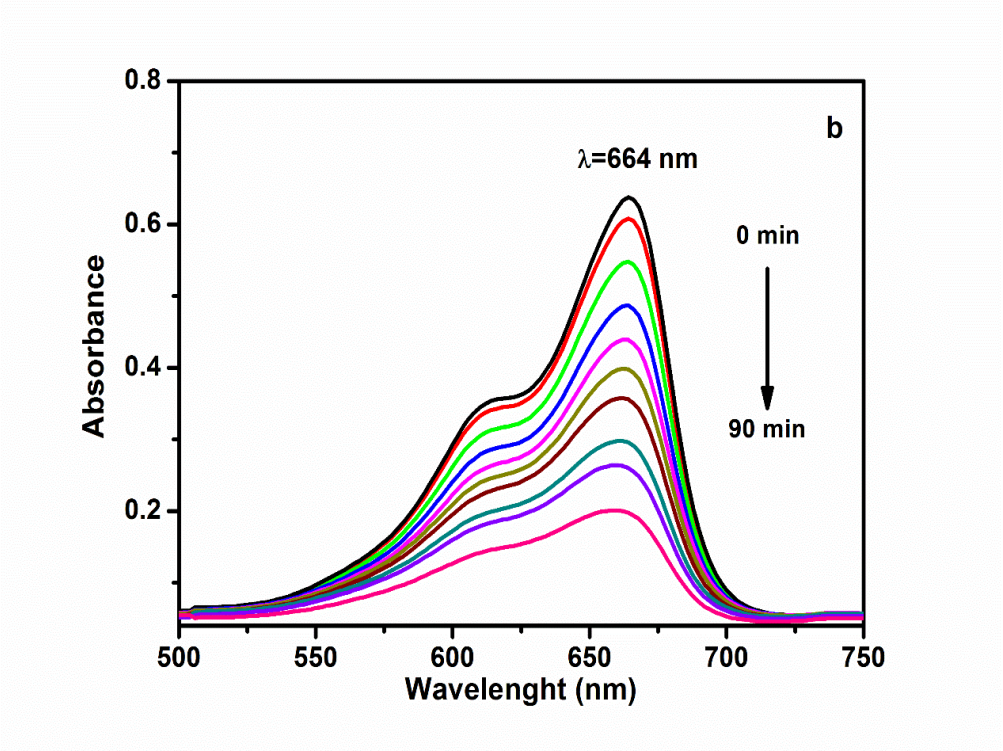
λ=664 nm
b
0 min
90 min
Absorbance
Wavelenght (nm)
0.8
0.6
0.4
0.2
500
550
600
650
700
750

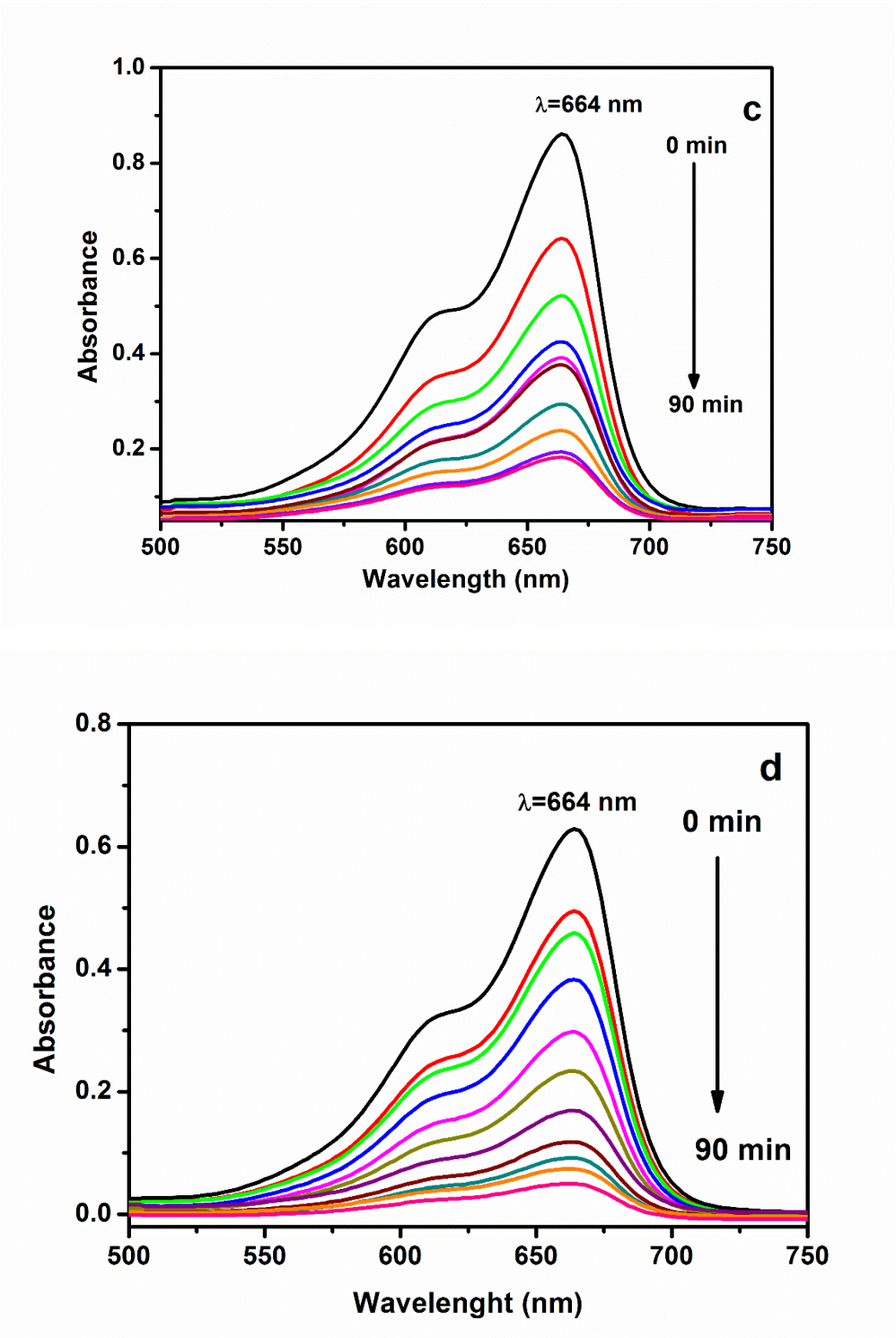

Fig. 8 Decay of the UV-Vis absorption spectrum of ($1.5X10^{-5}$ M) MB aqueous solution during UV irradiation in the presence of 50 mg (a) TiO_2, b) TiO_2/GO, c) 0.015 mol% Sm-TiO_2/GO and d) 0.015 mol% Eu-TiO_2/GO catalysts

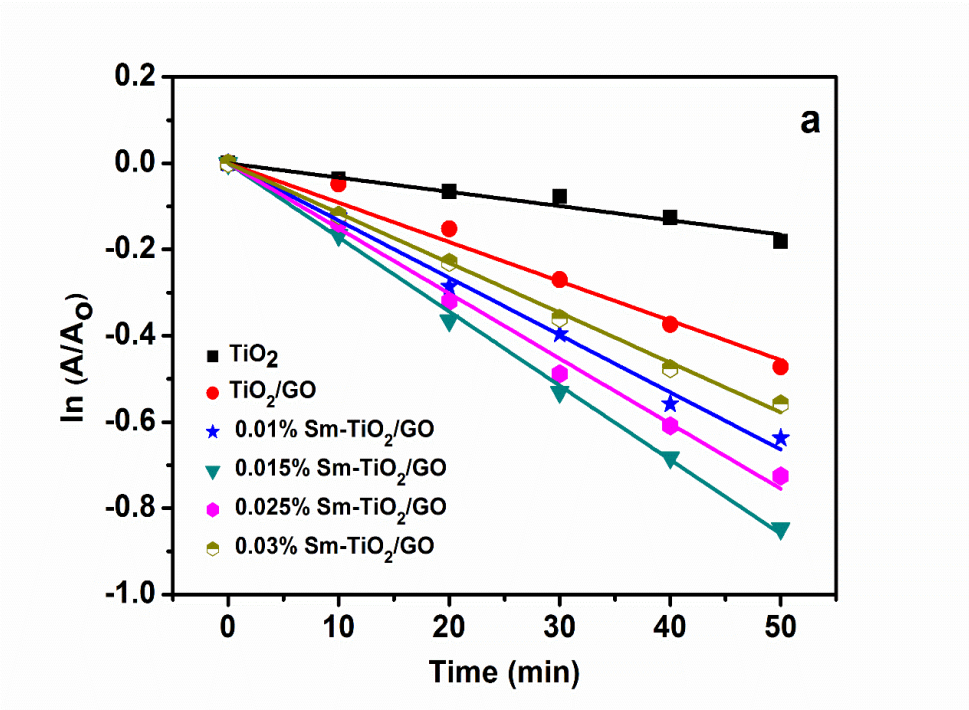
a
0.2
0.0
-0.2
-0.4
-0.6
-0.8
-1.0
ln (A/A$_O$)
0
10
20
30
40
50
Time (min)
TiO$_2$
TiO$_2$/GO
0.01% Sm-TiO$_2$/GO
0.015% Sm-TiO$_2$/GO
0.025% Sm-TiO$_2$/GO
0.03% Sm-TiO$_2$/GO

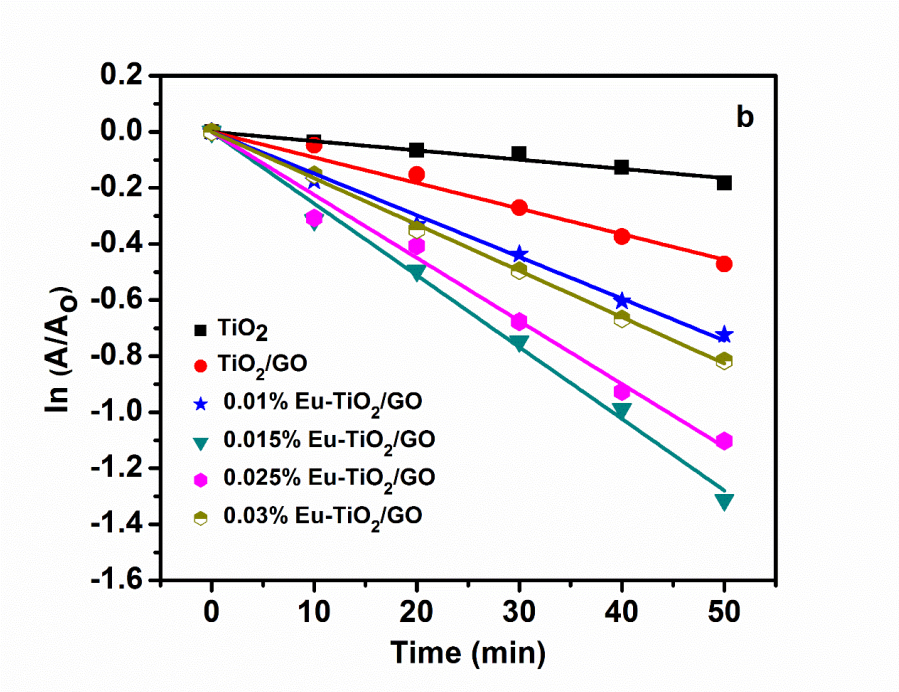
b
0.2
0.0
-0.2
-0.4
-0.6
-0.8
-1.0
-1.2
-1.4
-1.6
ln (A/A$_O$)
0
10
20
30
40
50
Time (min)
TiO$_2$
TiO$_2$/GO
0.01% Eu-TiO$_2$/GO
0.015% Eu-TiO$_2$/GO
0.025% Eu-TiO$_2$/GO
0.03% Eu-TiO$_2$/GO

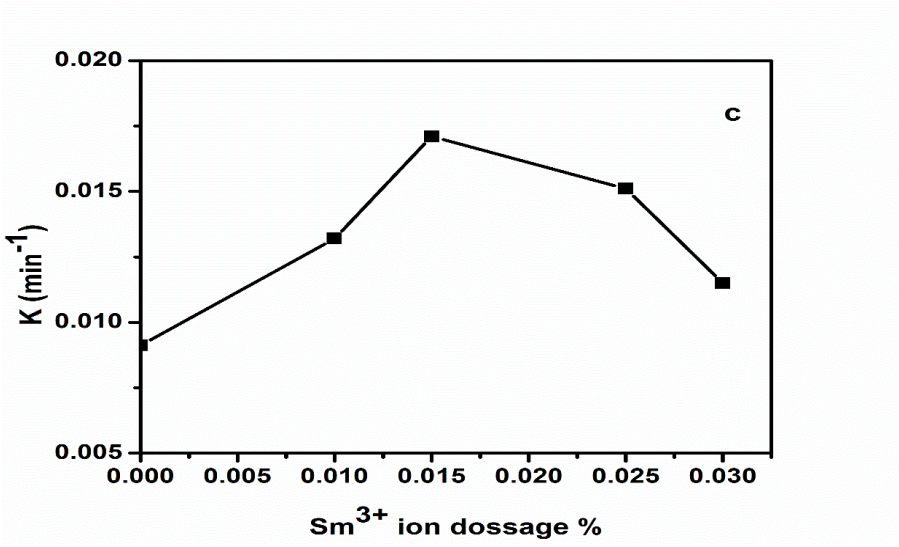

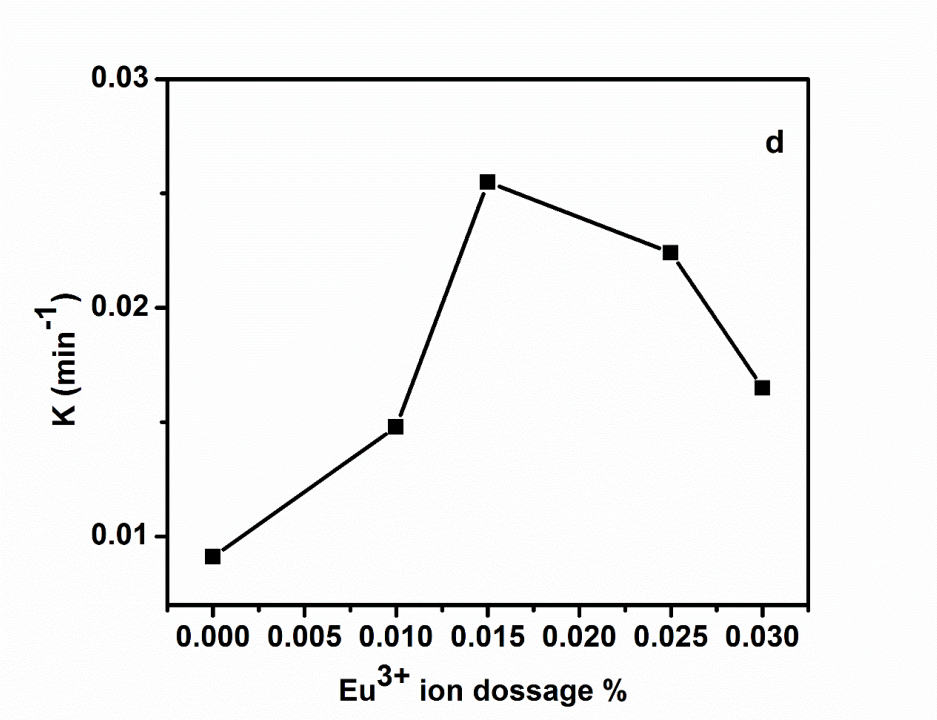

Fig. 9(a,b) 1st order rate kinetics of the photocatalytic degradation of 1.5×10^{-5} M aqueous solution of MB in the presence of 50 mg TiO_2, TiO_2/GO, x mol% Sm- TiO_2/GO and x mol% Eu- TiO_2/GO catalysts; Fig. 9(c, d) Influence of the different molar ratios of the Sm^{3+} and Eu^{3+} dopant ion conc. on the decolorization rate of MB

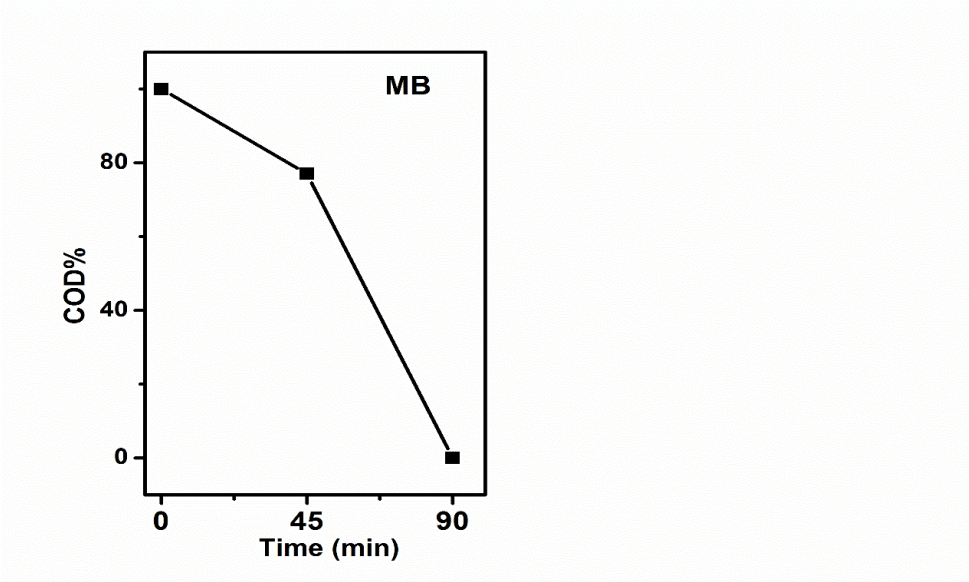

Fig. 10 COD% decay of MB dye solution under UV-illumination in the presence of 0.015% Eu^{3+}-TiO_2/GO photocatalyst

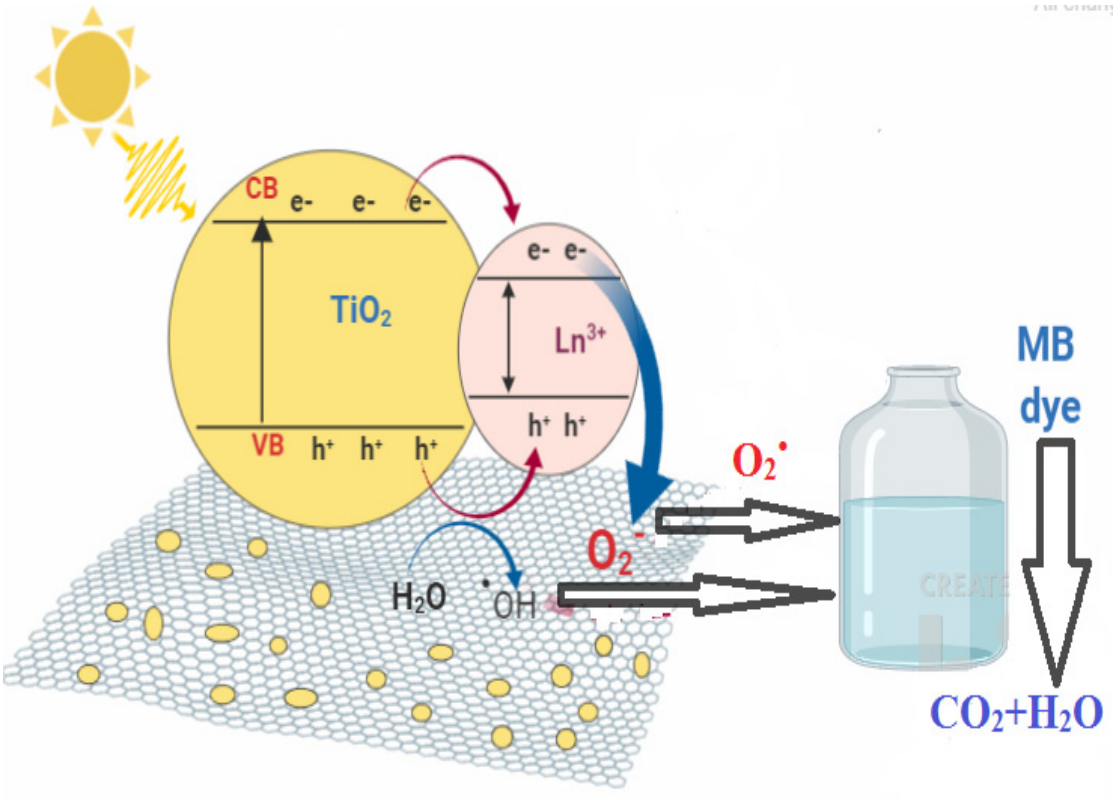

Fig. 11 Proposed mechanism of photocatalytic degradation of MB over Ln(III)-TiO_2/GO photocatalyst under UV irradiation

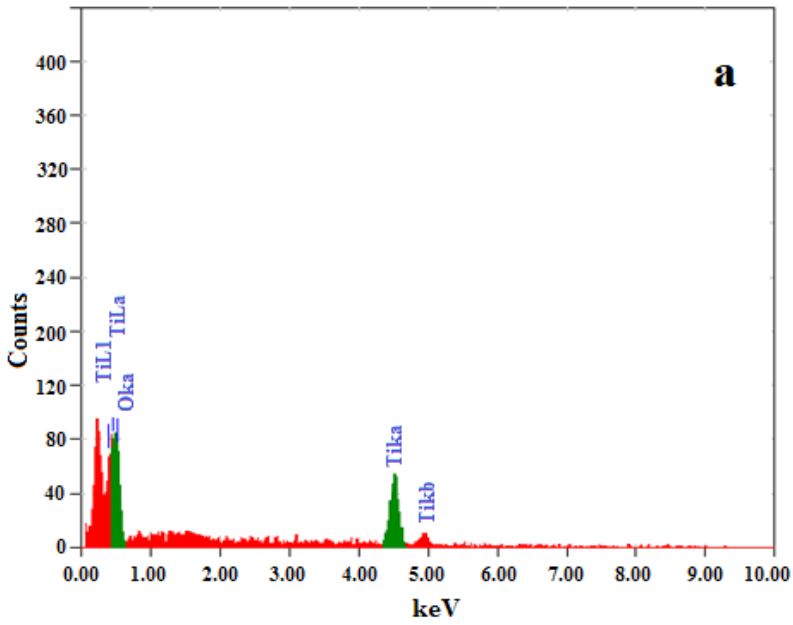
a
Counts
keV
TiL1
TiLa
Oka
Tika
Tikb

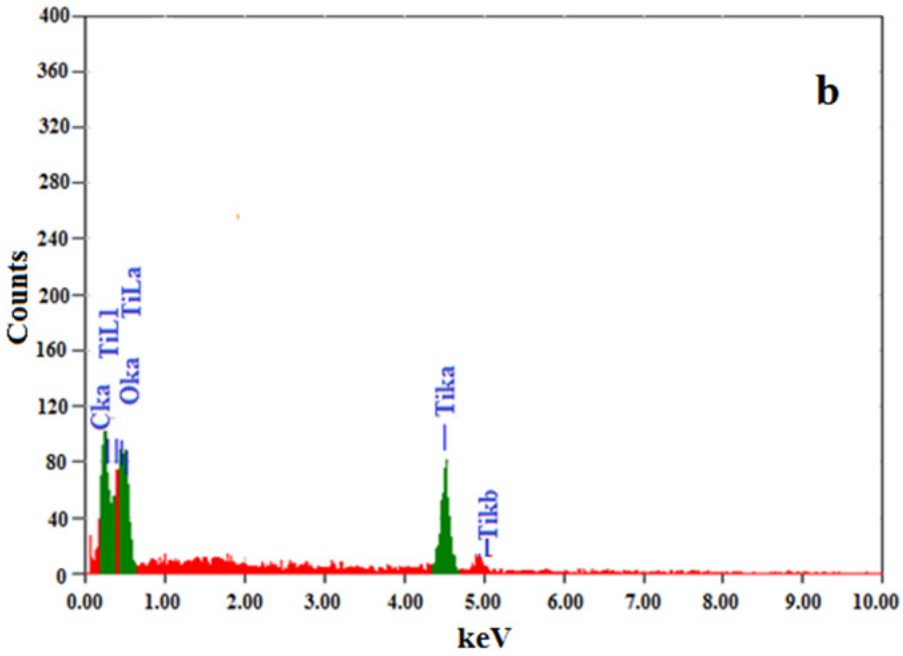
b
Counts
keV
Cka
TiL1
TiLa
Oka
Tika
Tikb

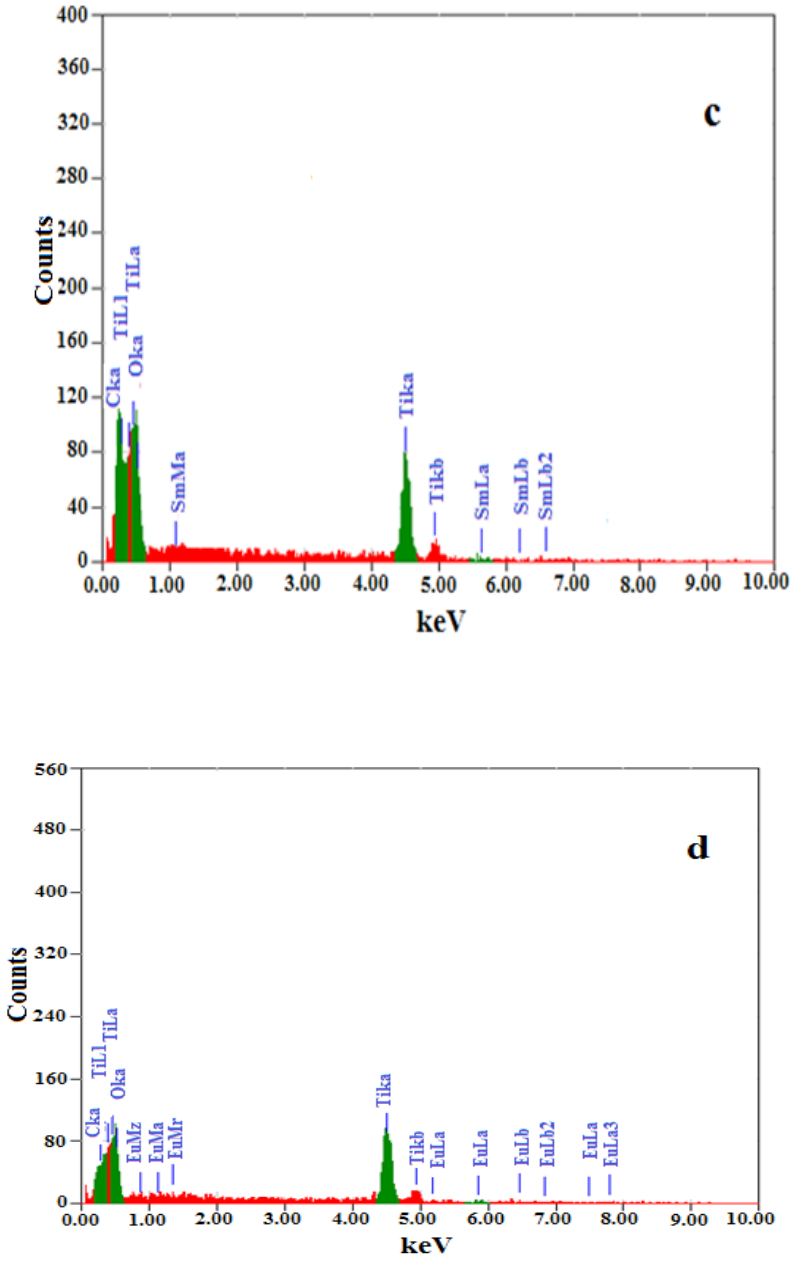

Supplement 1: EDX analysis of a) pure TiO_2, b) TiO_2/GO, 0.015% Sm-TiO_2/GO and d) 0.015% Eu-TiO_2/GO nanocomposite materials

of oxygen radicals prompting a decrease of the photocatalytic process [34]. Therefore, controlling the dose of metal dopants in the nanocomposites is an important factor for the enhancement of photocatalysis [35].

Mineralization Study

The photocatalytic activity of the highest active 0.015% Eu^{3+}-TiO_2/GO photocatalyst has been quantitatively assessed by measuring the COD% decay during the photodegradation experiments (Fig. 10). Fig. 10 indicates that 99.9% of COD was removed after only 90 min of UV-illumination. This (COD% removal) analysis confirms the potentiality of this photocatalytic nanomaterial to efficiently mineralize the MB organic dye pollutant.

Proposed Photocatalytic Mechanism:

The explanation of the enhancement of the photocatalytic activity of the prepared catalysts due to lanthanides doping and graphene oxide incorporation can be explained according to Equations (4-10) [18, 35]. Firstly, up on UV-light illumination, the excited TiO_2 particles generate electron-hole pairs (eq. 4). Then the photogenerated electrons excited from the valence band (VB) to the conduction band (CB) of TiO_2. Ln^{3+} dopant in TiO_2 act as electron scavenger and reduce their recombination with h^+ and produce Ln^{2+} (eq. 5) [36,37]. The produced Ln^{2+} ions are very unstable, so that e^- can be easily descavenged either by passing to the adsorb O_2 molecules (eq. 6), promoting $O_2^{\bullet}$ and $^{\bullet}OH$ formation or by transferring to GO as well to produce superoxide anion (eq. 7). The reactive superoxide radical ion ($O_2^{\bullet}$) can easily react with adsorbed water molecules to produce the very reactive oxidizing species ($^{\bullet}OH$) (eq. 8). On the other hand, the positive holes (h^+) in the TiO_2 valance band can also promote the MB degradation by either direct oxidation of MB or by generating ($^{\bullet}OH$) radicals (eq. 9). The powerful oxidizing species ($^{\bullet}OH$) can easily lead to degradation of MB dye (eq. 10). Moreover, the possible mechanism involved in the photocatalytic degradation of Ln(III) doped TiO_2/GO photocatalyst can be represented in Fig. 11.

$$TiO_2 \xrightarrow{UV\ (h\nu)} h^+_{VB} + e^-_{CB} \quad (4)$$

$$Ln^{+3} + (TiO_2)e^-_{CB} \rightarrow Ln^{+2} \quad (5)$$

$$(Ln^{+3})\ e^- + GO \rightarrow e^-(GO) \quad (6)$$

$$O_2 + e^-(GO) \rightarrow O_2^- \quad (7)$$

$$O_2^{-\bullet} + H_2O \rightarrow {}^{\bullet}OH \quad (8)$$

$$(TiO_2)\ h^+_{VB} + OH^- \rightarrow {}^{\bullet}OH \quad (9)$$

$$^{\bullet}OH + MB \rightarrow \text{degradation products} \quad (10)$$

Conclusion

Different molar ratios of Eu^{3+} and Sm^{3+}-doped TiO_2 loaded on GO nanocomposite photocatalysts were successfully prepared by a facile and low-cost hydrothermal method. The photocatalytic activity of the prepared Ln(III) nanocomposite photocatalysts was tested for the decolorization and degradation rate of methylene blue (MB) as a model of organic dye pollutants. The results clearly showed the beneficial role of both the GO and the lanthanide metal ions as a dopant on the degradability of MB. The high specific surface area of GO and its oxygen containing functional groups resulted in increase the absorptivity and hence the degradability of MB. The GO content acted as a photosensitizer and an electron scavenger to decrease the photogenerated electron–hole pair's recombination and in this way expand its absorbance in the visible region leading to a great photocatalytic activity. Doping the as-synthesized nanocomposite with an appropriate amount of Ln(III) metal ions such as Sm^{3+} and Eu^{3+} led to further enhancement in the photocatalytic activity of the TiO_2/GO and TiO_2 relatively and expanded the quantity of electron–hole pairs to take part in the photocatalytic reaction. The 0.015% Eu^{3+}-doped TiO_2/GO photocatalyst showed the highest photocatalytic activity. The high photocatalytic performance combined with its higher absorbance in the visible region confirmed the synergistic impacts of the Ln(III) dopants.

Conflict of interest

The authors declare that they have no conflict of interest regarding the publication of this paper.

Acknowledgment

This paper is extracted from a Ph.D. thesis submitted to the faculty of Science –Ain Shams University as partial fulfilment of the Ph.D. degree.

References

1. Boxue Z., Shengxin C., Meiqi D., Xiaozhou Y., Yun W. and Jianfeng Y., Titanium Dioxide (TiO_2) Mesocrystals: Synthesis Growth Mechanisms and Photocatalytic Properties. *Catalysts,* **9** (1), 1-27 (2019).

2. Ji L. Sh., Huimin H. and Xianjun L., Phenol–TiO_2 complex photocatalysis: visible light-driven selective oxidation of amines into

imines in air. *Sustainable Energy & Fuels,* **3** (2), 488- 498 (2019).

3. Andrea G., David M. T., Salvatore G. L., Billy J. M., Maria P. S., Martin A., Giovanni N. and Richard B., Sol gel graphene/TiO_2 nanoparticles for the photocatalytic-assisted sensing and abatement of NO_2. *Applied Catalysis B: Environmental,* **243**, 183-194 (2019).

4. Shindume L. H., Zhao Z., Wang N., Liu H., Umar A., Zhang J., Wu T. and Guo Z., Enhanced Photocatalytic Activity of B, N-Codoped TiO_2 by a New Molten Nitrate Process. *Journal of Nanoscience & Nanotechnology Research,* **19** (2), 839-849 (2019).

5. Kiran B., Nasir A., Irfan A. Sh. and Tayyaba M. A., Effects of Different Parameters on Photocatalytic Oxidation of Slaughterhouse Wastewater Using TiO_2 and Silver-Doped TiO_2 Nanoparticles. *Polish Journal of Environmental Studied,* **28** (3), 1591–1600 (2019).

6. Mona S. and Abdel-Mottaleb M. S.A., Titanium dioxide nanomaterial doped with trivalent lanthanide ions of Tb, Eu and Sm: Preparation, characterization and potential applications. *Inorganic Chimica Acta,* **360**, 2863–2874 (2007).

7. Joanna R. S., Tomasz G., Janusz W. S., Wojciech L., Maria G., Bunsho O. and Adriana Z., Lanthanide co-doped TiO_2: The effect of metal type and amount on surface properties and photocatalytic activity. *Applied Surface Science,* **307**, 333–345 (2014).

8. Charfeddine M., Taher G., Jalila J., Mondher G., Alanood A. A., Mounir G., Miguel M. S. and Hatem E., Synthesis and Characterization of SnO_2-TiO_2 Nanocomposites Photocatalysts. *Current Nanoscience,* **15** (4), 398 – 406 (2019).

9. Nejc R., David M. T., Uroš C., Harinarayanan P., João A. L., Andraž L. and Andrijana S. Š., Hydrothermal Synthesis of Rare-Earth Modified Titania: Influence on Phase Composition, Optical Properties, and Photocatalytic Activity. *Materials*, **12** (5), 1-19 (2019).

10. Feng Z., Chunjie Y., Qi S. and Sridhar K., TiO_2/Sepiolite nanocomposites doped with rare earth ions: Preparation, characterization and visible light photocatalytic activity. *Microporous and Mesoporous Materials*, **274**, 25-32 (2019).

11. Liu S. H. and Lin W. X., Simple method to prepare g-C_3N_4-TiO_2/waste zeolites as visible-light-responsive photocatalytic coatings for degradation of indoor formaldehyde. *Journal of Hazard Materials,* **368**, 468-476 (2019).

12. Olivia S., Robert L., Leslie B., Ivana J. Z., Azar F., Shasvat R., Peng P., Mark R.S. and Norman Y. Z., Photocatalytic Degradation of Microcystins by TiO_2 Using UV-LED Controlled Periodic Illumination. *Catalysts,* **9** (2), 1-10 (2019).

13. Ziming Z., Yu L., Sha L., Wei W. and Jiantai M., Preparation of a magnetic mesoporous Fe_3O_4–Pd@TiO_2 photocatalyst for the efficient selective reduction of aromatic cyanides. *New Journal of Chemistry,* **43** (16), 6294-6302 (2019).

14. Meicen G., Xiaocai Y., Jinghua L., Liping W., Zhiwei N. and Hang Y., Composite Photocatalysts of CNTS-TiO_2: An Efficient Photocatalyst for the Degradation of Ammonia Nitrogen Pollutant in Mariculture Wastewater under UV Light Irradiation. *IOP Conference Series: Materials Science and Engineering,* **301**, 1-8 (2018).

15. Mohammad B. A., Zoha T. B., Majid S., Sedigheh B. D. and Payam V., Synthesis of TiO_2 nanoparticles and decorated multi-wall carbon nanotube (MWCNT) with anatase TiO_2 nanoparticles and study of optical properties and structural characterization of TiO_2/MWCNT nanocomposite. *Optik*, **149**, 447–454 (2017).

16. Yongfang Y., Lidong X., Hefang W., Wenjie W. and Lixin Z., TiO_2/graphene porous composite and its photocatalytic degradation of methylene Blue. *Materials & Design*, **108**, 632-639 (2016).

17. Daniela M., Dmitry K., Jacob B., Alexander S., Zhengzong S., Alexander S., Lawrence A., Wei L. and James T., Improved Synthesis of Graphene Oxide. *ASC Nano*, **8** (4) 4806-4814 (2010).

18. Shizhen L., Hongqi S., Shaomin L. and Shaobin W., Graphene facilitated visible light

photodegradation of methylene blue over titanium dioxide photocatalysts. *Chemical Engineering Journal*, **214**, 298-303 (2013).

19. Leila Sh. and Anjali A., Graphene Oxide Synthesized by using Modified Hummers Approach. *International* Journal *of Electrical Engineering and Electronics,* **2** (1), 58-63 (2014).

20. Tingting L., Yong G., Junwo Z., Manying Z., Xiaofei F. and Fang L. A., Membrane Modified with Nitrogen-Doped TiO_2/ Graphene Oxide for Improved Photocatalytic Performance. *Applied Sciences,* **9** (5), 1-12 (2019).

21. Samuel O., William A., Sudheesh Sh. and Poomani G., Lanthanum doped–TiO_2 decorated on graphene oxide nanocomposite: A photocatalyst for enhanced degradation of acid blue 40 under simulated solar light. *Advanced Material Lett*ers, **8** (3) 295-302 (2017).

22. Cullity B. D., Stock S. R., Elements of X-ray Diffractio, 2nd Ed. addision-Wesley publishing company INC. California (2001).

23. Shinya H., Titanium Dioxide Based Visible Light Sensitive Photocatalysis: Mechanistic Insight and Applications. *Catalysts*, **9** (2), 1-22 (2019).

24. Jun Ch. L., Anantha I. G., Gopalan S. A., Kwang P. L. and Wha J. K., Preparation of Visible Light Photocatalytic Graphene Embedded Rutile Titanium (IV) Oxide Composite Nanowires and Enhanced NO_x Removal. *Catalysts*, **9** (2) 1-18 (2019).

25. Tingting L., Yong G., Junwo Z., Manying Z., Xiaofei F. and Fang L. A., Membrane Modified with Nitrogen-Doped TiO_2/ Graphene Oxide for Improved Photocatalytic Performance. *Applied Sciences,* **9** (5), 1-12 (2019).

26. Shizhen L., Hongqi S., Shaomin L. and Shaobin W., Graphene facilitated visible light photodegradation of methylene blue over titanium dioxide photocatalysts. *Chemical Engineering J*ournal, **214**, 298-303 (2013).

27. Yu L. M., Kan Z., Wei Z., Fang C. Z., You C. Ch. and Yuan G. Z., Enhanced chemical interaction between TiO_2 and graphene oxide for photocatalytic decolorization of methylene blue. *Chemical Engineering J*ournal*,* **193–194**, 203–210 (2012).

28. Martins P. M., Ferreira C. G., Silva A. R., Magalhães B., Alves M. M., Pereira L., Marques P. A. A. P., Melle F. M. and Lanceros M. S., TiO_2/graphene and TiO_2/graphene oxide nanocomposites for photocatalytic Applications: A computer modeling and experimental study. *Composites Part B*: *Engineering*, **145**, 39-46 (2018).

29. Poonam B., Manish K., Pankaj Ch. and Kamal K. K., Enhanced photocatalytic degradation of methylene blue and adsorption of arsenic(III) by reduced graphene oxide (rGO)–metal oxide (TiO_2/Fe_3O_4) based nanocomposites. *RSC*, **5** (89)73249–73260 (2015).

30. Thuy P., Viet P., Eun Sh., Hai P., Sun K., Jin Ch., Eui K. and Seung H., The role of graphene oxide content on the adsorption-enhanced photocatalysis of titanium dioxide graphene oxide composites. *Chemical Engineering J*ournal, **170**, 226-232 (2011).

31. William V., Angie R., Carlos D. U., Carlos G. and Patricia Q., Photocatalytic activity of graphene oxide – TiO_2 thin films sensitized by natural dyes extracted from Bactrisguineensis. *RSC*, **6** (3), 1-17 (2019).

32. Amr T., Adham R. R. and Omar A. El., Di-oxide/Graphene and Titanium Dioxide/Graphene Oxide Nanocomposites: Synthesis, Characterization and Photocatalytic Applications for Water Decontamination. *Catalysts,* **8** (11), 1-45 (2018).

33. Feizpoor S., Habibi Y. A. and Vadivel S., Novel TiO_2/Ag_2CrO_4 nanocomposites: efficient visible–light-driven photocatalysts with n–n heterojunctions. *Journal of Photochemistry* and *Photobiology*, **341**, 57-68 (2017).

34. Sakthivel S., Shankar M. V., Palanichamy M., Arabindoo B., Bahnemann D. W. and Murugesan V., Enhancement of photocatalytic activity by metal deposition: characterisation and photonic efficiency of Pt, Au and Pd deposited on TiO_2 catalyst. *Water Research*, **38** (13), 3001-3008 (2004).

35. Davis E. A. and Mott N. F., Conduction in

non-crystalline systems V. Conductivity, optical absorption and photoconductivity in amorphous semiconductors. *The Philosophical Magazine: A Journal of Theoretical Experimental and Applied Physics*, **22** (179), 903-922 (1970).

36. Venkata R. P., Viswadevarayalu V. A. and Adinarayana R. S., Fabrication of graphene–TiO_2 nanocomposite with improved photocatalytic degradation for acid orange 7 dye under solar light irradiation. *Bulletin of Materials Sci*ence, **39** (3), 759- 767 (2016).

37. Ali Z., Chaudhry M. N., Niaz N. A., Khalid N. R., Ahmed E., Hussain R., Ahmed I., Abbas S. M., Significant effect of Graphene on catalytic degradation of Methylene blue by pure and Ce-doped TiO_2 at nanoscale. *Digest Journal of Nanomaterials and Biostructures*, **8** (4), 1525-1535 (2013).

38. Khalid N. R., Ahmed E., Zhanglian H. and Ahmed M., Synthesis and photocatalytic properties of visible light responsive La/TiO_2-graphene composites. *Applied Surface Science,* **263**, 254–259, (2012).

تحضير حرارى سهل لاكسيد التيتانيوم النانومتري المطعم بالساماريوم والايروبيم والمحمل على اكسيد الجرافين وإستخدامها كحفازات ضوئية فعالة.

مريم شاكر جوهر[1]*, هدى سعيد حافظ[2], منى مصطفى سيف[3], هشام محمد عبد الفتاح سليمان[1], محمد صبري أحمد عبد المطلب[4]

[١] قسم المواد النانومترية والمتراكبات الجديدة - معهد بحوث التكنولوجيا المتقدمة والمواد الجديدة - مدينة الابحاث العلمية والتطبيقات التكنولوجيا- برج العرب الجديدة – ص.ب. ٢١٩٣٤ – الاسكندرية – مصر.

[٢] معهد البحوث والدراسات البيئية – جامعة المنوفية فرع السادات – السادات - مصر.

[٣] قسم الكيمياء – كلية التربية- جامعة عين شمس- ص.ب. ١١٣٤١- القاهرة- مصر.

[٤] قسم الكيمياء – كلية العلوم – جامعة عين شمس- ص.ب. ١١٥٦٦- القاهرة – مصر.

تم تحضير لاكسيد التيتانيوم المطعم بأيونات الساماريوم والايروبيم وحمل على أكسيد الجرافين بطريقة حرارية بسيطة. تم دراسة الخواص التركيبية والمورفولوجية والضوئية للتركيبات النانوية بواسطة جهاز حيود الأشعة السينية (XRD)، الفحص المجهري الإلكتروني (SEM) المجهز بأشعة أشعة تشتت الطاقة (EDX)،والمجهر الإلكتروني (TEM)،وتحليل مساحة السطح (SBET)، وتحليل فورية الطيفي للأشعة تحت الحمراء (FTIR)،و مطياف رامان (RS) ، ومطياف الانعكاس المنتشر (DRS). وتم التحقيق من الكفاءة الحفزية الضوئية للعينات المحضرة بقدرتها على إزالة لون صبغة الميثيلين الأزرق (MB) كنموذج لملوثات الصبغ العضوية وذلك بواسطة الأشعة فوق البنفسجية. وتظهر نتائج التحفيز الضوئي أن متراكب نانو $0.015\ mol\%\ Eu^{3+}$- TiO_2/GO ذو نشاط تحفيزي ضوئي عالى من حيث الكفاءة في إزالة اللون وتكسيرالصبغة. مما يوضح أن هذه المادة النانوية المركبة الجديدة المطعمة بأيونات اللانثينيدات تعتبر محفز ضوئي واعد لتكسير ملوثات الأصباغ العضوية في المحاليل المائية. وقد أظهر تحليل الطلب على الأكسجين الكيميائي (COD) درجة عالية من التمعدن الكامل لصبغة الميثلين الازرق بعد ٩٠ دقيقة فقط تحت ضوء الأشعة فوق البنفسجية.